Intermetallics 167 (2024) 108212

Contents lists available at ScienceDirect

Intermetallics

journal homepage: www.elsevier.com/locate/intermet

Fast cooling rate enhances impact toughness in tungsten fiber-reinforced metallic glass composites

Y.Z. Wu [a,b,1], C.B. Jin [b,1], M.Y. Tan [b], F.C. Wang [b], Y.H. Gao [b], J. Xu [b], Z.W. Shao [c], Z. Ren [c], Y. Zhang [b], J.Q. Wang [b,**], J.T. Huo [b,***], M. Gao [b,*]

[a] School of Materials Science and Chemical Engineering, Ningbo University, Ningbo, 315211, China
[b] CAS Key Laboratory of Magnetic Materials and Devices, Zhejiang Province Key Laboratory of Magnetic Materials and Application Technology, Ningbo Institute of Materials Technology and Engineering, Chinese Academy of Sciences, Ningbo, 315201, China
[c] Ningbo Branch, Ordnance Science Institute of China, Ningbo, 315103, China

ARTICLE INFO

Keywords:
Metallic glass composite
Tungsten fiber
Suction casting
Cooling rate
Rejuvenation
Impact toughness

ABSTRACT

Ex-situ second-phase reinforced metallic glass composites (MGCs) hold great promise as damage-tolerant structural materials for practical applications. However, limitations in fabrication techniques have hindered significant improvements in MGC toughness. In this study, we introduce a novel experimental approach that employs suction casting technology with adjustable cooling rates to fabricate tungsten fiber-reinforced MGCs. The impact toughness of MGCs exhibits a direct correlation with the volume fraction of tungsten fibers, reaching its peak value of 42J/cm^2 at a 16 % volume fraction. Notably, MGCs subjected to faster cooling rates demonstrate superior impact toughness compared to their slow-cooled counterparts. This enhancement can be primarily attributed to the rejuvenation effect and the resulting increase in fracture toughness within the MG matrix, a direct consequence of the faster cooling rate. The current research presents an innovative methodology for enhancing MGC toughness through the rejuvenation of the MG matrix.

1. Introduction

As one typical kind of amorphous materials, metallic glasses (MGs) are known for their exceptional physical and chemical properties [1–5]. Notably, their remarkable mechanical characteristics, including high specific strength, substantial elastic strain, and considerable fracture toughness, have garnered considerable attentions [4,6,7]. However, in addition to these mechanical properties, practical applications demand robust dynamic mechanical properties, particularly high impact toughness [7,8]. Unlike fracture toughness, which measures a material's resistance to crack propagation, impact toughness assesses its ability to undergo permanent deformation and absorb plastic deformation energy during impact events. In crystalline materials, impact toughness is closely associated with various structural defects, such as point defects, dislocations, and grain boundaries [9–11]. In contrast, MGs lack these structural defects. The absence of multiscale structural defects renders MGs exceptionally strong but relatively-brittle, resulting in lower impact toughness compared to their crystalline counterparts [12]. Thus, the enhancement of impact toughness is pivotal for promoting the practical applications of MGs.

Plastic deformation in MGs primarily depends on the formation, interaction, and propagation of shear bands (SBs) [13–15]. The scarcity of SBs and rapid SB propagation significantly limits intrinsic plastic deformation capabilities, resulting in reduced ductility and toughness in most MGs. Recent research has highlighted that the introduction of the second phase in MGs can enhance plastic deformation capabilities by activating multiple SBs and constraining SB propagation [16–20]. A similar experimental strategy based on MG composites (MGCs) has been employed to improve impact toughness [21–25]. However, the impact toughness of MGCs still lags significantly behind that of crystalline alloys [12]. Tungsten fiber-reinforced Zr-based MGC represents the pioneering amorphous matrix composite and has found applications in the military due to its outstanding self-sharpening properties [21,23]. The introduction of tungsten fibers, owing to their high hardness and

* Corresponding author.
** Corresponding author.
*** Corresponding author.
E-mail addresses: jqwang@nimte.ac.cn (J.Q. Wang), huojuntao@nimte.ac.cn (J.T. Huo), gaomeng@nimte.ac.cn (M. Gao).
[1] These authors contributed equally to this work.

https://doi.org/10.1016/j.intermet.2024.108212
Received 11 December 2023; Received in revised form 23 January 2024; Accepted 28 January 2024
Available online 3 February 2024

density, is considered a promising method to enhance the mechanical properties of MGCs. However, the conventional preparation method for tungsten fiber-reinforced MGCs relies on pressure penetration and water quenching [21–24]. Due to excessively slow cooling rates, this method usually leads to the crystallization of amorphous matrix and severely limits improvements in impact toughness of MGCs [12,21–23]. Additionally, several studies have demonstrated a positive correlation between fracture toughness and impact toughness in various metallic materials [26–28]. Hence, enhancing the intrinsic fracture toughness of the MG matrix stands as a crucial factor in improving the impact toughness of tungsten fiber-reinforced MGCs.

In this work, we proposed a novel strategy of increasing the cooling rate during suction casting to enhance the fracture toughness of the MG matrix and substantially improve the impact toughness of tungsten fiber-reinforced MGCs. We observed that impact toughness increases with both the volume fraction of tungsten fibers and the applied cooling rate. The detailed physical mechanisms behind these enhancements were systematically discussed.

2. Experimental methods

The nominal composition of $Zr_{61}Ti_2Cu_{25}Al_{12}$ (at.%) (ZT1) was selected as the MG matrix due to its substantial intrinsic fracture toughness and excellent glass-forming ability [29]. An ingot corresponding to this composition was produced through arc melting a mixture of 99.99 % pure metals in a high-purity argon atmosphere. To ensure chemical homogeneity, the ingot underwent at least six remelting cycles, resulting in a minimal mass loss of less than 0.3 %. The obtained ingot was then sectioned into smaller pieces. In the subsequent steps, several tungsten fibers with the diameter of 400 μm and the length of 65 mm were positioned vertically in the center of a copper mold. Before placing the tungsten fibers, all of the fibers were carefully cleaned. First, the ultrasonic cleaning within alcohol was applied to remove surface oils. Then, a series of sandpapers were used to slightly grind and remove the oxide layer. Finally, the second round of ultrasonic cleaning was conducted to eliminate any remaining impurities. The ingot pieces were placed on top of the copper mold, and the molten material was drawn into the mold through arc melting. Finally, a tungsten fiber-reinforced MGC cylinder with a 5 mm diameter and a 55 mm length was prepared.

The microstructure and morphology of the MGC samples were characterized using X-ray diffraction (XRD, Bruker D8), scanning electron microscopy (SEM, ZEISS EVO18), and energy dispersive X-ray spectroscopy (EDS, ZEISS EVO18). In accordance with the international standard GB/T 229–2020, impact tests were conducted using an impact instrument (Congyue JWB) with a maximum hammer speed of 5.3 m/s and a maximum impact energy of 450 J. The MGC samples used in the impact tests were un-notched and had dimensions of 5 mm × 55 mm (diameter × length). Three samples were tested under identical experimental conditions to determine the average impact toughness and the corresponding error bars were calculated for each MGC. The fracture toughness of the MG matrix was primarily determined through nanoindentation tests using a Bruker TI980 nanoindenter (detailed methods can be found in the Supplementary Material). The indenter tip employed was the Berkovich type and the curvature radius was approximately 100 nm. For the nanoindentation tests, the rod samples were firstly cut into several slices with the thickness of 2 mm. Then, these slices were put into the rubber molds and the mixture of epoxy resin and hardener was poured into the molds for an 8h curing process. Subsequently, all of the mounted samples undergo progressive polishing procedures using polishing cloths and the particle sizes of the polishing suspensions were 15, 6, 3, 1, 0.5, and 0.1 μm, respectively.

3. Results and discussion

3.1. Characterization of the structure and morphology for tungsten fiber-reinforced MGCs

Fig. 1(a) illustrates the preparation process of the resulting tungsten fiber-reinforced MGCs using copper mold suction casting technology. Fig. 1(b) displays the optical image of one MGC sample. The cooling rate during MGC casting was controlled by adjusting the cyclic cooling water temperature ranging between 20 and 30 °C. Specifically, we employed 20 °C for rapid cooling and 30 °C for slow cooling. Due to the superior thermal conductivity of the copper mold and the effect of cyclic cooling water, the obtained MG matrix during suction casting retains a completely amorphous structure, as confirmed by the XRD result in Fig. 1(c). Consequently, this method offers an improved approach for achieving a fully amorphous MG matrix in tungsten fiber-reinforced MGCs compared to the prior method involving pressure penetration and water quenching [21–24].

It's worth noting that suction casting is an uncommon method for preparing MGCs considering that volume shrinkage of the melt during fast cooling leads to inadequate bonding between tungsten fibers and the MG matrix. To assess the bonding between the tungsten fibers and MG matrix, we examined the cross-sectional morphology of an MGC sample (denoted as ZT1-9.6 %W, where 9.6 % represents the volume fraction of tungsten fibers within the MGC) in Fig. 2(a). Clearly, there are no noticeable pores or cracks between the tungsten fibers and the MG matrix, indicating a strong bonding. What is more, we selected a local region delineated by a yellow dashed rectangle in Fig. 2(a) for a detailed quantitative analysis of the tungsten fiber-MG matrix interface, as presented in Fig. 2(b). Elemental distributions within this region in Fig. 2(c) reveal tungsten exclusively in the tungsten fibers and there is no evidence of a diffusion reaction between tungsten and the MG matrix. Furthermore, other elements are homogeneously distributed, indicating no segregation of chemical elements. Additionally, we conducted EDS linear scanning along the red dashed line in Fig. 2(b), as shown in Fig. 2(d). An interface is evident between the tungsten and the MG matrix, with a spacing of 0.4 μm. The continuous evolution of various elements along the red dashed line implies the absence of pore formation during rapid cooling.

3.2. Effect of the volume fraction of tungsten fibers on the impact toughness of MGCs

To investigate the effect of the volume fraction of tungsten fibers on the impact toughness of MGCs, we incorporated varying numbers of tungsten fibers (0, 5, 15, 25, 30) into the MG matrix and a series of MGCs were prepared. The corresponding volume fractions of tungsten fibers within MGCs were 0, 3.2 %, 9.6 %, 16 %, and 19.2 %, respectively. We labeled these MGC samples as ZT1, ZT1-3.2 %W, ZT1-9.6 %W, ZT1-16 %W, and ZT1-19.2 %W. From Fig. 2, S1(a) and S1(b), when the volume fraction of tungsten fibers is below 19.2 %, no pores or defects are observed within the MGCs. However, when the volume fraction reaches approximately 19.2 %, various pores with different sizes and shapes appear at the interface between the tungsten fibers and the MG matrix (see Fig. S1(c)). This result indicates that the melt fails to fill the space between the tungsten fibers and the copper mold when the volume fraction of tungsten fibers exceeds a critical value. Consequently, our current experimental apparatus requires enhancement to mitigate this limitation, which will be our focus in the subsequent research phase.

Fig. 3(a) illustrates the setup for Charpy no-notch impact tests and the lower part displays the fixed MGC rod. Following the standard Charpy impact principle, we can determine the impact work corresponding to the impact fracture of each MGC sample. Detailed impact toughness values are listed in Table 1 and plotted in Fig. 3(b). Notably, the impact toughness of MGCs increases with increasing volume fraction of tungsten fibers. At a volume fraction of approximately 16 %, the

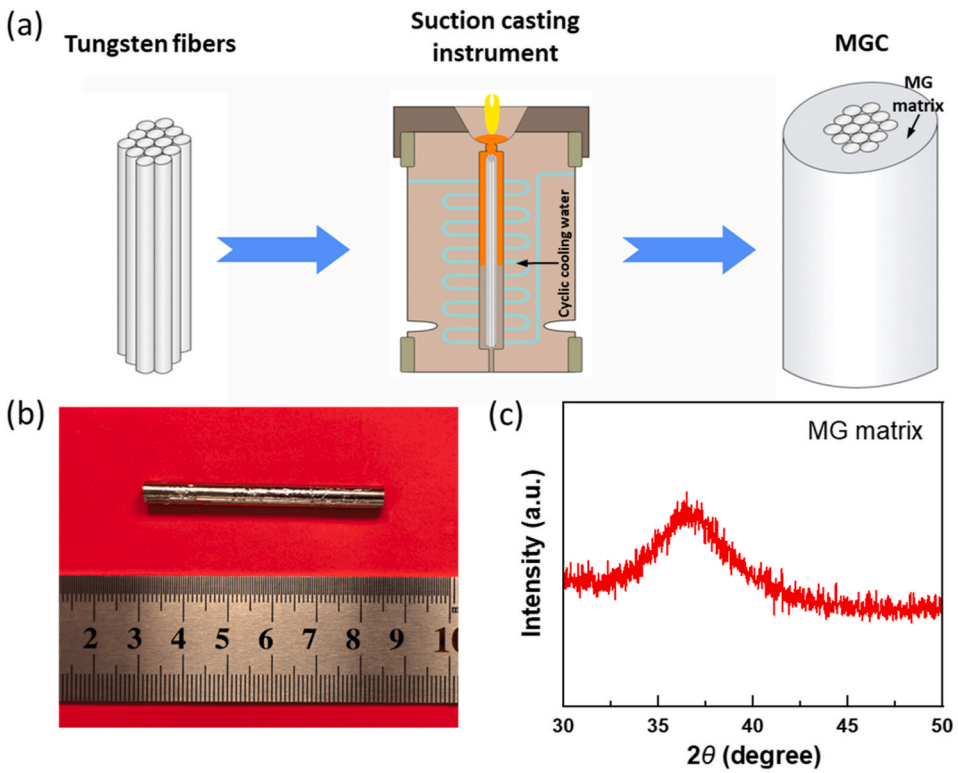

Fig. 1. (a) Scheme of the preparation procedure for tungsten fiber-reinforced MGCs using suction casting. (b) Optical image of one tungsten fiber-reinforced MGC. (c) X-ray diffraction pattern of the MG matrix in tungsten fiber-reinforced MGC.

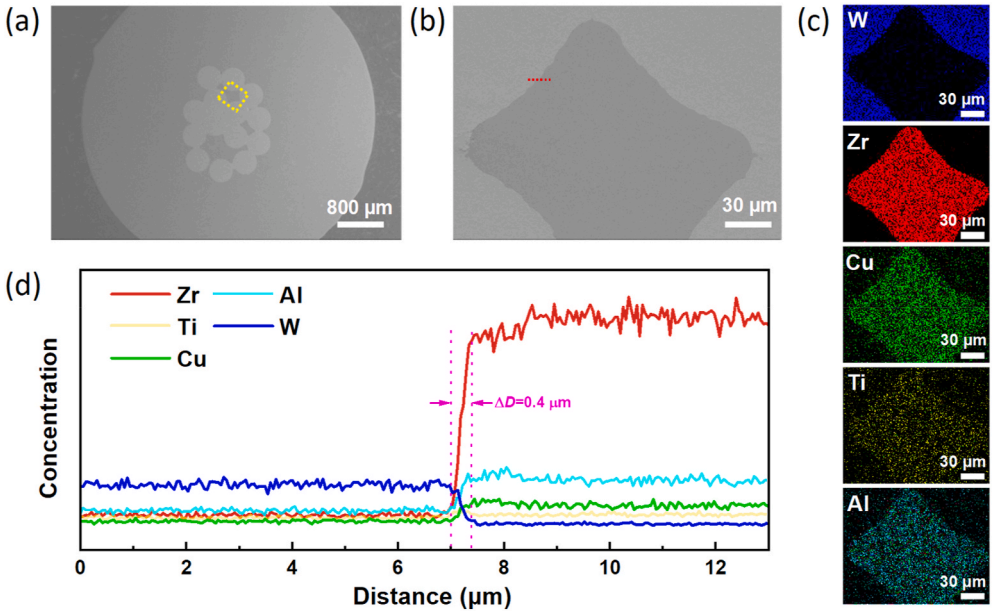

Fig. 2. (a) SEM image of the cross-section of the tungsten fiber reinforced MGC sample (ZT1-9.6 %W, 9.6 % is the volume fraction of the tungsten fibers within the MGC, fast cooling rate). (b) Enlarged SEM image of the local region marked by the yellow dashed square in Fig. 1(a). The red dashed line points out the transition from the tungsten fiber to the MG matrix. (c) EDS images of the spatial distribution for different elements corresponding to the local region marked by the yellow dashed square in Fig. 1(a). (d) Plot of the concentration evolution of different elements along the red dashed line in Fig. 1(b).

impact toughness peaks at 42 J/cm^2. Further increasing the volume fraction from 16 % to 19.2 % results in a decrease in impact toughness to 39 J/cm^2. Prior research reported that higher volume fractions of tungsten fibers correspond to higher impact toughness when MGCs exhibit no pores or defects [12,21–24]. Combining these results with the SEM findings in Fig. 2 and Fig. S1, the decrease in impact toughness for the ZT1-19.2 %W sample is primarily attributed to the appearance of various pores at the interfaces between the tungsten fibers and the MG matrix. Therefore, it is expected that upgrading the experimental instrument to prevent pore formation during suction casting could increase the impact toughness of MGCs based on the current experimental strategy in this work.

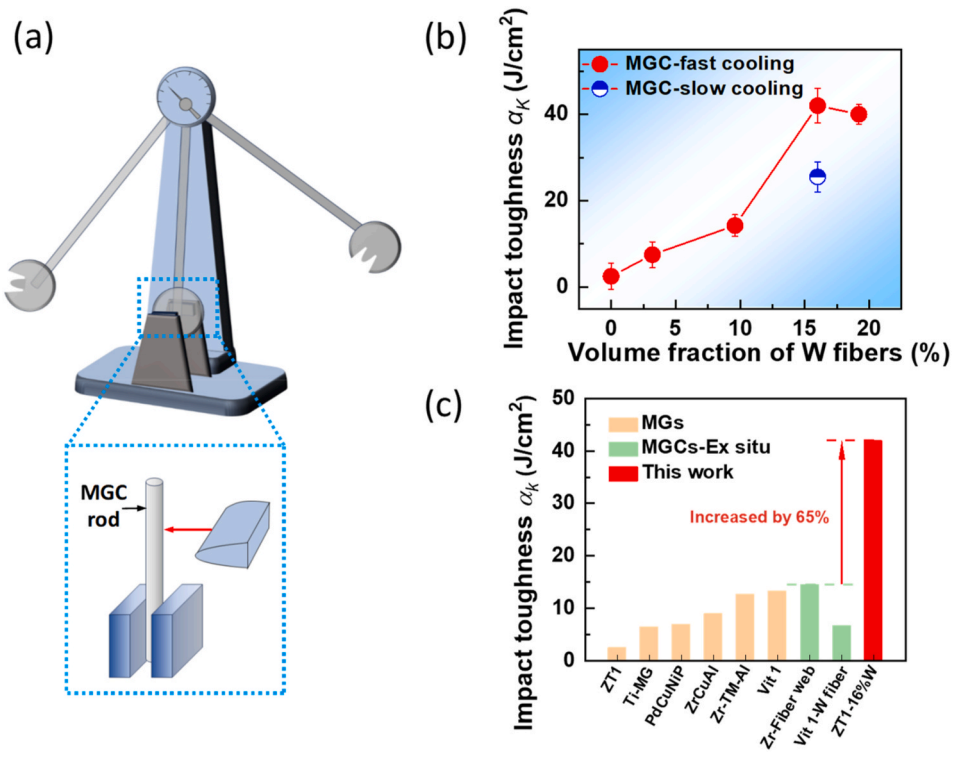

Fig. 3. (a) Scheme of the applied impact tests on the tungsten fiber reinforced MGC. The blue dashed rectangle gives the detailed setup for the hammer tip and the sample. (b) Plot of the impact toughness and the volume fraction of the tungsten fibers. The red and blue colors represent the applied fast and slow cooling rates, respectively. (c) Comparison histogram of fracture toughness for fast and slow cooled MGCs. The inset shows the positive relationship between the fracture toughness and the impact toughness. (d) Impact toughness comparison of various materials reported in different years. The red arrow shows the 30 % increase of the impact toughness for the ZT1-16 %W MGC compared to the previous reported maximum value.

Table 1
Impact toughness and the corresponding volume fraction of the tungsten fibers for MGCs in this study.

Volume fraction of W fibers (%)		Impact toughness α_k (J/cm^2)
0		2.5
3.2		7.5
9.6		14.3
16	slow cooling	25.5
	fast cooling	42
19.2		40

3.3. Effect of cooling rate on the impact toughness of MGCs

The intrinsic toughness of the MG matrix in MGCs significantly affects their impact mechanical properties. Different cooling rates typically result in MGs with varying toughness properties [30,31]. In this study, we selected two cooling water temperatures, 20 °C and 30 °C, to achieve two different cooling rates. Specifically, we prepared the MGC sample ZT1-16 %W using a slow cooling rate with higher cooling water temperature. The corresponding impact toughness for ZT1-16 %W with the slow cooling rate is also presented in Fig. 2(b). Compared to ZT1-16 %W with a fast cooling rate, the impact toughness drops from 42 J/cm^2 to 25.5 J/cm^2. Thus, there is a positive correlation between the applied cooling rate and the impact toughness of MGCs.

To investigate how the cooling rate affects the physical properties of the MG matrix in MGCs, we conducted a series of DSC measurements and nanoindentation tests on MG matrix subjected to fast and slow cooling rates. Fig. 4(a) shows two typical heat flow curves for MG matrix samples. Both of heat flow curves exhibit clear relaxation signals before the glass transition. However, the overall heats during relaxation (recovery enthalpy) before the glass transition under slow and fast cooling rates are significantly different. The recovery enthalpy for the fast-cooled MG matrix is 9.83 J/g and is much larger than the 1.12 J/g for the slow-cooled MG matrix. This result directly implies that the fast-cooled MG matrix is in a higher energy state compared to the slow-cooled MG matrix. Nanoindentation tests were also employed to determine the elastic modulus of the MG matrix and the detailed results were exhibited in Fig. 4(b). The detailed nanoindentation load and displacement curves were also included in the insertion of Fig. 4(b). Obviously, the elastic modulus of the fast-cooled MG matrix is smaller than that of the slow-cooled MG matrix. Based on the free volume model of MGs [1], the fast-cooled MG matrix possesses more free volumes than the slow-cooled MG matrix, which is consistent with the higher recovery enthalpy. Furthermore, the presence of more free volume within the MG matrix makes MGCs exhibit better plasticity and greater toughness.

Furthermore, we utilized an experimental estimation method based on nanoindentation to study the effect of cooling rate on the intrinsic toughness of the MG matrix. The detailed estimation procedure can be seen in the Supplementary Material. The values of fracture toughness for the MG matrix under fast and slow cooling rates are shown in Fig. 4(c). Clearly, the fracture toughness of the MG matrix under the fast cooling rate, 132 MPa m$^{1/2}$, is much larger than that of the MG matrix under the slow cooling rate, 85 MPa m$^{1/2}$. This finding suggests that faster cooling rate enhances the intrinsic toughness of the MG matrix. Additionally, a positive relationship exists between fracture toughness, recovery enthalpy for the MG matrix, and impact toughness of MGCs, as demonstrated in Fig. 4(d). It should be noted that a similar positive relationship between fracture toughness and impact toughness has been reported in crystalline materials [26–28]. Consequently, our research suggests that by improving the intrinsic toughness of the MG matrix, the impact toughness of MGCs can be significantly enhanced.

To compare the impact resistance of the MGCs developed in this study with other MGCs prepared by ex-situ methods, we summarized the values of impact toughness for various ex-situ phase reinforced MGCs

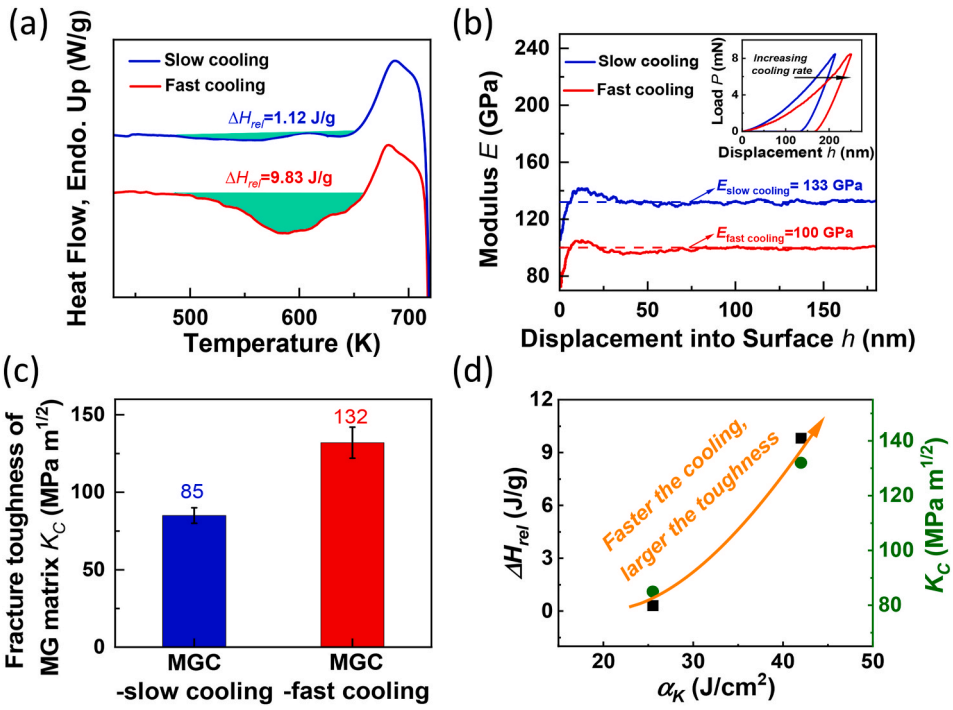

Fig. 4. (a) Heat flow curves for MG matrix within the MGCs by different cooling rates. The green shaded regions give the overall heat of the relaxation before the glass transition. (b) Modulus comparison for MG matrix within the MGCs by different cooling rates. The inserted plot gives the typical nanoindentation load and displacement curves for MG matrix within the MGCs by different cooling rates. (c) Comparison histogram of fracture toughness of MG matrix for fast and slow cooled MGCs. (d) Plot of the impact toughness for MGCs, the relaxation heat and the fracture toughness for MG matrix with different cooling rates.

[12,32–38] in Table 2 and displayed in Fig. 3(c). As reference materials, we also included the impact toughness values for several MGs in Fig. 3 (c). Clearly, the impact toughness of ZT1-16 %W MGC with a fast cooling rate in this study is the highest at 42 J/cm^2 compared to other ex-situ phase reinforced MGCs and MGs. For instance, ZT1 MG exhibits a small impact toughness of only 2.5 J/cm^2. When tungsten fibers and a high cooling rate are applied, the impact toughness of ZT1-16 %W MGC increases by a factor of 16.8. Furthermore, compared to previous Zr-Fiber web reinforced MGCs, the impact toughness was improved by 65 %. Conversely, for Vit 1, a typical MG with significant practical potential, its impact toughness surpasses that of Vit 1-W fiber reinforced MGC counterpart prepared by previous method of pressure penetration and water quenching. The decrease in impact toughness for Vit 1-W fiber reinforced MGC may be attributed to the low cooling rate during pressure penetration and water quenching. It is expected that the impact toughness for Vit 1-W fiber reinforced MGC can be improved by increasing the cooling rate, as demonstrated in our experimental strategy.

Table 2
Summary of the impact toughness of MGs and MGCs by Ex-situ methods.

System	Composition	Impact toughness α_K (J/cm^2)	Reference
MGs	$Zr_{61}Ti_2Cu_{25}Al_{12}$ (ZT1)	2.5	This work
	$Pd_{40}Cu_{30}Ni_{10}P_{20}$	7	[31]
	$Zr_{59}Cu_{31}Al_{10}$	9	[32]
	$Zr_{41.2}Ti_{13.8}Cu_{12.5}Ni_{10}Be_{22.5}$ (Vit 1)	13.3	[33]
	$Zr_{64}Hf_{1.5}Nb_3Cu_{13}Ni_{11}Al_{7.5}$ (Zr-TM-Al)	12.7	[34]
	$(Ti_{41}Zr_{25}Be_{26}Ni_8)_{93}Cu_7$ (Ti-MG)	6.5	[35]
MGCs (Ex-situ method)	Vit 1-W fiber	6.7	[36]
	$Zr_{63.36}Cu_{14.52}Ni_{10.12}Al_{12}$-Fiber web	14.57	[37]
	ZT1-16 %W	42	This work

3.4. Comparison analyses of surface and fracture morphology for MGCs with different cooling rates after impact tests

To elucidate the physical mechanism behind the difference in impact toughness for tungsten fiber reinforced MGCs subjected to different cooling rates, we systematically analyzed the corresponding surface and fracture morphology for two ZT1-16 %W MGCs with fast and slow cooling rates. As shown in Fig. 5(a) and (b), distinct shear band (SB) patterns are evident on the surfaces of fast-cooled and slow-cooled MGCs (inserted optical photos show the post-impact surface morphology). In the fast-cooled MGC (Fig. 5(a)), multiple SBs form during impact, and the SB propagation direction exhibits pronounced turning. In contrast, slow-cooled MGCs display only two primary SBs, with no significant turning for the SB propagation direction. The presence of multiple SBs and the change in SB propagation direction align with the larger fracture toughness of fast-cooled MG matrix, as depicted in Fig. 4(c). In Fig. 5(c) and (d), the fracture morphology for fast-cooled and slow-cooled MGCs exhibits similar characteristics. After impacts, cracks and fissures appear between the tungsten fibers and the MG matrix. The main distinction is that the fracture surface on the MG matrix for fast-cooled MGCs appears rougher than that of slow-cooled MGCs. For a detailed examination, we selected two local regions on the fracture surfaces of fast and slow-cooled MGCs marked by red dashed rectangles in Fig. 5(c) and (d). The enlarged SEM images of the marked regions are displayed in Fig. 5 (e) and (f). Both fracture surfaces for fast-cooled and slow-cooled MGCs exhibit dimple-like patterns, indicative of ductile fracture mechanisms [39,40]. Notably, the typical size of the dimple structure for fast-cooled MGCs appears larger than that of slow-cooled MGCs.

For a quantitative characterization of the dimple structures on the fracture surfaces of fast-cooled and slow-cooled MGCs, the probability distributions of dimple structure sizes based on Fig. 5(e) and (f), are shown in Fig. 5(g) and (h). Clearly, the peak size (D_p) of dimple structures for fast-cooled MGCs is 16 μm. While D_p for slow-cooled MGCs is approximately 8 μm, representing a two-fold reduction in size. For MGs, larger dimple structures are typically associated with greater fracture

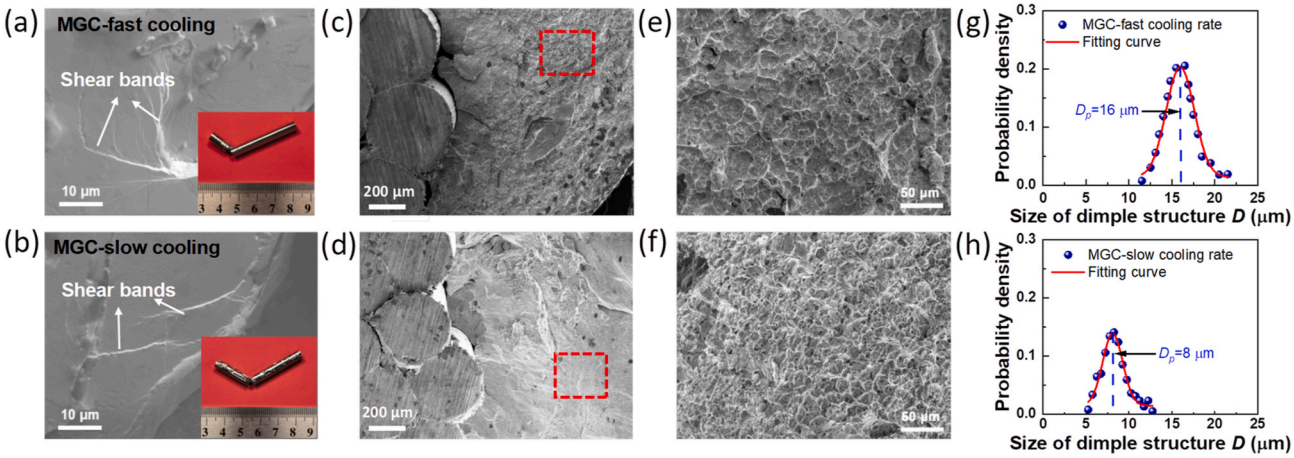

Fig. 5. (a) Surface morphology after the impact test for ZT1-16 %W MGCs with fast cooling. (b) Surface morphology after the impact test for ZT1-16 %W MGCs with slow cooling rate. The inserted optical pictures show the sample condition after the impact tests. The white arrows point out the formed shear bands on the MGC sample surface. (c) Fracture morphology for ZT1-16 %W MGC with fast cooling. (d) Fracture morphology for ZT1-16 %W MGC with slow cooling. The red dashed rectangles mark the typical fracture region. (e) Enlarged SEM images for the marked region in Fig. 5(c). (f) Enlarged SEM images for the marked region in Fig. 5(d). (g) Probability density function for the size of dimple-like structures correspond to Fig. 5(e). (h) Probability density function for the size of dimple-like structures correspond to Fig. 5(f).

toughness [41]. Hence, the larger average size of dimple structures suggests greater fracture toughness in the MG matrix of fast-cooled MGC being consistent with the above results of the estimated fracture toughness in Fig. 4(c).

Notably, our research demonstrates that faster cooling rates can significantly enhance the impact toughness of tungsten fiber-reinforced MGCs by increasing the fracture toughness of the MG matrix. From the perspective of the potential energy landscape [42–44], MGs produced with faster cooling rates occupy higher energy states than those produced with slower cooling rates. In other words, faster cooling rates can elevate MGs to higher energy states, representing an experimental strategy for rejuvenating MGs [45–48]. Consequently, our results imply that the rejuvenation of the MG matrix by faster cooling rates can effectively enhance the impact toughness of MGCs. However, due to limitations in the current suction casting method, the rejuvenation effect in our study remains constrained and should be further improved through instrument upgrades. For example, reducing the cooling water temperature or substituting cooling water with liquid nitrogen may enhance the rejuvenation effect of the current strategy. Additionally, other post-processing techniques such as shock compression, cyclic loading, or non-affine thermal strain may further boost the impact toughness of MGCs by rejuvenating the MG matrix. It should be noted that the experimental strategy introduced in this work may be employed for the fabrication of other metal-matrix composites. For example, fast cooling rate can refine the microscopic grain structures and obviously improve the mechanical properties of the high entropy alloys and Al alloys [49,50]. Thus, by applying the suction casting method to prepare the composites with the matrix of high entropy alloy or Al alloy, the obtained composite samples may own the superior mechanical properties compared to the slow cooled ones. This topic will be included in our research plan.

4. Conclusions

In conclusion, this study introduces a novel method for preparing tungsten fiber-reinforced MGCs using suction casting, resulting in crack and pore-free composites. The systematic investigation into the influence of tungsten fiber volume fraction and cooling rate on the impact toughness of the MGCs was conducted. It was found that the impact toughness of MGCs displays a gradual increase with increasing tungsten fiber volume fractions. Specifically, when the volume fraction of tungsten fibers reaches 16 %, the impact toughness peaks at 42 J/cm^2. However, a further increase in the volume fraction to 19.2 % leads to the reduced impact toughness due to the formation of pores at the interface between the tungsten fiber and the MG matrix. What is more, MGCs subjected to a faster cooling rate exhibit superior impact toughness compared to their slow-cooled counterparts. This effect can be attributed to the increased intrinsic fracture toughness of MG matrix under faster cooling rates, which enables the MGCs to generate multiple shear bands and resist rapid shear band propagation. These findings not only shed light on the rejuvenation effect induced by a faster cooling rate on the toughness of MGs but also offer guidance for enhancing the impact toughness of MGCs by rejuvenating the MG matrix.

CRediT authorship contribution statement

Y.Z. Wu: Writing – original draft, Methodology, Investigation. **C.B. Jin:** Validation, Methodology, Investigation, Formal analysis. **M.Y. Tan:** Validation, Formal analysis, Data curation. **F.C. Wang:** Validation. **Y.H. Gao:** Validation, Formal analysis. **J. Xu:** Validation. **Z.W. Shao:** Methodology, Formal analysis. **Z. Ren:** Validation. **Y. Zhang:** Validation. **J. Q. Wang:** Writing – review & editing, Funding acquisition, Conceptualization. **J.T. Huo:** Writing – review & editing, Resources, Project administration, Funding acquisition. **M. Gao:** Writing – review & editing, Supervision, Project administration, Funding acquisition, Conceptualization.

Declaration of competing interest

The authors declare that they have no known competing financial interests or personal relationships that could have appeared to influence the work reported in this paper.

Data availability

Data will be made available on request.

Acknowledgments

This work was supported by the National Natural Science Foundation of China (52201194, 52222105, 92163108, 52231006), 3315 Innovation Youth Talent in Ningbo City (2021A123G), Youth Innovation Promotion Association CAS (No. 2019296), Zhejiang Provincial Natural Science Foundation of China (LR22E010004), Zhejiang Provincial

Natural Science Foundation Regional Innovation and Development Joint Foundation with Quzhou City (LZY23E010002).

Appendix A. Supplementary data

Supplementary data to this article can be found online at https://doi.org/10.1016/j.intermet.2024.108212.

Supplementary materials

Supplementary material associated with this article can be found.

References

[1] C.A. Schuh, T.C. Hufnagel, U. Ramamurty, Mechanical behavior of amorphous alloys, Acta Mater. 55 (2007) 4067–4109.
[2] W.H. Wang, Bulk metallic glasses with functional physical properties, Adv. Mater. 21 (2009) 4524–4544.
[3] M.W. Chen, A brief overview of bulk metallic glasses, NPG Asia Mater. 3 (2011) 82–90.
[4] J.J. Kruzic, Bulk metallic glasses as structural materials: a review, Adv. Eng. Mater. 18 (2016) 1308–1331.
[5] J. Howard, K. Carlson, D. Chidambaram, High-temperature metallic glasses: status, needs, and opportunities, Phys. Rev. Mater. 5 (2021) 040301.
[6] M.M. Trexler, N.N. Thadhani, Mechanical properties of bulk metallic glasses, Prog. Mater. Sci. 55 (2010) 759–839.
[7] L. Wondraczek, E. Bouchbinder, A. Ehrlicher, J.C. Mauro, R. Sajzew, M. M. Smedskjaer, Advancing the mechanical Performance of glasses: Perspectives and Challenges, Adv. Mater. 34 (2021) 2109029.
[8] D. C Hofmann, S.N. Roberts, Microgravity metal processing: from undercooled liquids to bulk metallic glasses, NPJ Microgravity 1 (2015) 15003.
[9] Y. Lin, Q. Yu, J. Pan, F.H. Duan, R.O. Ritchie, Y. Li, On the impact toughness of gradient-structured metals, Acta Mater. 193 (2020) 125–137.
[10] L. Lei, Y.Q. Zhao, Q.Y. Zhao, C. Wu, S.X. Huang, W.J. Jia, W.D. Zeng, Impact toughness and deformation modes of Ti-6Al-4V alloy with different microstructures, Mater. Sci. Eng. A 801 (2021) 140411.
[11] Y.H. Wang, Y.B. Zhang, A. Godfrey, J.M. Kang, Y. Peng, T.S. Wang, N. Hansen, X. X. Huang, Cryogenic toughness in a low-cost austenitic steel, Comm. Mater. 2 (2021) 44.
[12] G. Yin, F.W. Li, L. Deng, J.S. Jin, P. Gong, Research status and prospect of impact toughness of amorphous alloys, Chin. J. Nonferrous Met. 30 (2020) 530–541.
[13] A.L. Greer, Y.Q. Cheng, E. Ma, Shear bands in metallic glasses, Mater. Sci. Eng. R Rep. 74 (2013) 71–132.
[14] R. Maaß, J.F. Löffler, Shear-band dynamics in metallic glasses, Adv. Funct. Mater. 25 (2015) 2353–2368.
[15] H.B. Zhou, L.Q. Shen, B.A. Sun, W.H. Wang, Research progress on the shear band of metallic glasses, J. Alloys Compd. 955 (2023) 170164.
[16] D.C. Hofmann, Jin-Yoo Suh, A. Wiest, G. Duan, Mary-Laura Lind, M.D. Demetriou, W.L. Johnson, Designing metallic glass matrix composites with high toughness and tensile ductility, Nature 451 (2008) 1085–1089.
[17] Y. Wu, Y.H. Xiao, G.L. Chen, C.T. Liu, Z.P. Lu, Bulk metallic glass composites with transformation-mediated work-hardening and ductility, Adv. Mater. 22 (2010) 2770–2773.
[18] W.J. Gao, W.W. Zhang, T. Zhang, C. Yang, X.S. Huang, Z.Y. Liu, Z. Wang, W.H. Li, W.R. Li, L. Li, L.H. Liu, Large tensile plasticity in Zr-based metallic glass/stainless steel interpenetrating-phase composites prepared by high pressure die casting, Compos. B 224 (2021) 109226.
[19] Y. F Ma, X.F. Tang, X. Wang, M. Zhang, H. Hu, P. Gong, X.Y. Wang, Preparation and mechanical properties of tungsten-particle-reinforced Zr-based bulk-metallic-glass composites, Mater. Sci. Eng. A. 815 (2021) 141312.
[20] T.Y. Yan, L. Zhang, Y. Wu, B. Li, H.M. Fu, H. Li, Y.W. Wang, X.W. Cheng, H. F. Zhang, Non-monotonic influence of cryogenic thermal cycling on rejuvenation and impact toughness of Ti-based bulk metallic glass composites, Scr. Mater. 228 (2023) 115340.
[21] R.B. Dandliker, R.D. Conner, W.L. Johnson, Melt infiltration casting of bulk metallic-glass matrix composites, J. Mater. Res. 13 (1998) 2896–2901.
[22] Z.M. Wang, H.G. Shi, H.W. Feng, F.J. Shang, L.J. Zhu, J.H. Su, Impact property of W fiber reinforced amorphous composite material, Ordnance Mater. Sci. Eng. 34 (2) (2011) 77–79.
[23] S. Roberts, C. Zachrisson, H. Kozachkov, A. Ullah, A.A. Shapiro, W.L. Johnson, D. C. Hofmann, Cryogenic Charpy impact testing of metallic glass matrix composites, Scr. Mater. 66 (5) (2012) 284–287.
[24] J.H. Chen, Y. Chen, M.Q. Jiang, X.W. Chen, H.F. Zhang, L.H. Dai, On the compressive failure of tungsten fiber reinforced Zr-based bulk metallic glass composite, Int. J. Solids Struct. 69–70 (2015) 428–441.
[25] X.Y. Cuan, Y. Lin, Z.H. Liu, B. Zhang, N. Li, J. Pan, On the impact toughness of amorphous/crystalline metallic laminates, J. Mater. Res. Technol. 26 (2023) 3756–3767.
[26] G. Terán, S. Capula-Colindres, D. Angeles-Herrera, J.C. Velázquez, M.J. Fernández-Cueto, Estimation of fracture toughness KIC from Charpy impact test data in T-welded connections repaired by grinding and wet welding, Eng. Fract. Mech. 153 (2016) 351–359.
[27] R.J. Smith, A.J. Horn, A.H. Sherry, Relating Charpy energy to fracture toughness in the lower transition region using a Weibull stress dependent energy scaling model, Int. J. Pres. Ves. Pip. 166 (2018) 72–83.
[28] H.F. Li, Q.Q. Duan, P. Zhang, X.H. Zhou, B. Wang, Z.F. Zhang, The quantitative relationship between fracture toughness and impact toughness in high-strength steels, Eng. Fract. Mech. 211 (2019) 362–370.
[29] Q. He, J.K. Shang, E. Ma, J. Xu, Crack-resistance curve of a Zr-Ti-Cu-Al bulk metallic glass with extraordinary fracture toughness, Acta Mater. 60 (2012) 4940–4949.
[30] W. Chen, H.F. Zhou, Z. Liu, J. Ketkaew, N. Li, J. Yurko, N. Hutchinson, H.J. Gao, J. Schroers, Processing effects on fracture toughness of metallic glasses, Scr. Mater. 130 (2017) 152–156.
[31] H. Li, Q.-X. Pei, Z.-D. Sha, P.S. Branicio, Intrinsic and extrinsic effects on the fracture toughness of ductile metallic glasses, Mech. Mater. 162 (2021) 104066.
[32] Y. Yokoyama, N. Nishiyama, K. Fukaura, H. Sunada, A. Inoue, Rotating-beam fatigue strength of $Pd_{40}Cu_{30}Ni_{10}P_{20}$ bulk amorphous alloy, Mater. Trans. 40 (1999) 696–699.
[33] Y. Yokoyama, T. Yamasaki, M. Nishijima, A. Inoue, Drastic increase in the toughness of structural relaxed hypoeutectic $Zr_{59}Cu_{31}Al_{10}$ bulk glassy alloy, Mater. Trans. 48 (2007) 1276–1281.
[34] R. Raghavan, P. Murali, U. Ramamurty, Ductile to brittle transition in the $Zr_{41.2}Ti_{13.75}Cu_{12.5}Ni_{10}Be_{22.5}$ bulk metallic glass, Intermetallics 14 (2006) 1051–1054.
[35] Y.H. Zhu, Z.W. Zhu, S. Chen, H.M. Zhang, H. Li, A.M. Wang, H.F. Zhang, Simultaneously enhancing strength and toughness of Zr-based bulk metallic glasses via minor Hf addition, Intermetallics 118 (2020) 106685.
[36] J.L. Gu, G.N. Yang, P. Gong, Y. Shao, K.F. Yao, Cryogenic charpy impact toughness of $(Ti_{41}Zr_{25}Be_{26}Ni_8)_{93}Cu_7$ bulk metallic glass, Mater. Sci. Eng. A 786 (2020) 139442.
[37] Z.M. Wang, H.G. Shi, H.W. Feng, F.J. Shang, L.J. Zhu, J.H. Su, Impact property of W fiber reinforced amorphous composite material, Ord. Mater. Sci. Eng. 34 (2011) 77–79.
[38] C. Xu, Preparation and Properties of Bulk Amorphous and its Composite Materials, Lanzhou University of Technology, Master of Science, 2013.
[39] M. Gao, B.A. Sun, C.C. Yuan, J. Ma, W.H. Wang, Hidden order in the fracture surface morphology of metallic glasses, Acta Mater. 60 (2012) 6952–6960.
[40] M. Gao, X.F. Cao, D.W. Ding, B.B. Wang, W.H. Wang, Decoding flow unit evolution upon annealing from fracture morphology in metallic glasses, Mater. Sci. Eng. A 686 (2017) 65–72.
[41] X.K. Xi, D.Q. Zhao, M.X. Pan, W.H. Wang, Y. Wu, J.J. Lewandowski, Fracture of brittle metallic glasses: Brittleness or plasticity, Phys. Rev. Lett. 94 (2005) 125510.
[42] W.L. Johnson, M.D. Demetriou, J.S. Harmon, M.L. Lind, K. Samwer, Rheology and ultrasonic properties of metallic glass-forming liquids: a potential energy landscape perspective, MRS Bull. 32 (2007) 644–650.
[43] X.X. Li, J.G. Wang, H.B. Ke, C. Yang, W.H. Wang, Extreme rejuvenation and superior stability in a metallic glass, Mater, Today Phys 27 (2022) 100782.
[44] Z.Z. Wang, P. Huang, X.L. Fan, F. Wang, Heterogeneity dependent cryogenic thermal cycling behavior of metallic glasses: a potential energy landscape perspective, Intermetallics 159 (2023) 107935.
[45] S.V. Ketov, Y.H. Sun, S. Nachum, Z. Lu, A. Checchi, A.R. Beraldin, H.Y. Bai, W. H. Wang, D.V. Louzguine-Luzgin, M.A. Carpenter, A.L. Greer, Rejuvenation of metallic glasses by non-affine thermal strain, Nature 524 (2015) 200–203.
[46] G. Ding, C. Li, A. Zaccone, W.H. Wang, H.C. Lei, F. Jiang, Z. Ling, M.Q. Jiang, Ultrafast extreme rejuvenation of metallic glasses by shock compression, Sci. Adv. 5 (2019) eaaw6249.
[47] J. Pan, Yu P. Ivanov, W.H. Zhou, Y. Li, A.L. Greer, Strain-hardening and suppression of shear-banding in rejuvenated bulk metallic glass, Nature 578 (2020) 559–562.
[48] W. Zhai, X.D. Hui, Y. Xiao, J.C. Qiao, S.L. Wei, T. Wang, L.H. Nie, B.B. Wei, Structural rejuvenation and toughening of bulk metallic glass via ultrasound excitation technique, Sci. China Tech. Sci. 63 (2020) 2395–2402.
[49] H. Huang, Y. Sun, P.P. Cao, Y. Wu, X.J. Liu, S.H. Jiang, H. Wang, Z.P. Lu, On cooling rates dependence of microstructure and mechanical properties of refractory high-entropy alloys HfTaTiZr and HfNbTiZ, Scr. Mater. 211 (2022) 114506.
[50] Marcella G.C. Xavier, Brenda J.M. Freitas, Guilherme L. Gouveia, Amauri Garcia, José E. Spinelli, The roles of Ni and Co in dendritic growth and tensile properties of Fe-Containing Al–Si–Cu–Zn scraps under slow and fast solidification cooling, Adv. Eng. Mater. 24 (2022) 2100822.